Cosmic Masers: Proper Motion toward the Next-Generation Large Projects
Proceedings IAU Symposium No. 380, 2024
T. Hirota, H. Imai, K. Menten, & Y. Pihlström, eds.
doi:10.1017/S1743921323002429

A comprehensive model of maser polarization

Boy Lankhaar

Department of Space, Earth and Environment, Chalmers University of Technology, Onsala Space Observatory, 439 92 Onsala, Sweden. email: lankhaar@chalmers.se

Abstract. Maser polarization observations have been successfully used to characterize magnetic fields towards a variety of astrophysical objects. Circular polarization yields the magnetic field strength of the maser source, and linear polarization yields information on the magnetic field morphology. Linear polarization can be produced when the maser saturates or through its anisotropic pumping. We present a comprehensive model of the polarization of masers. In contrast to regular excitation modeling, we relax the assumption of isotropically populated level populations, and model both the total population and level alignments. Through this approach, we obtain quantitative estimates on the anisotropic pumping of a variety of maser sources. In this way, the maser polarization may be related to the gas density, temperature, geometry and the magnetic field. Using the results of our modeling, we discuss, and give predictions, of the polarization of SiO, methanol, and water (mega)masers.

Keywords. masers, polarization, magnetic fields, stars: formation, stars: evolved

1. Introduction to maser polarization

Masers are prone to produce polarized radiation. While circular polarization is produced through the Zeeman effect, linear polarization is produced through the interaction of the maser molecules with the directional radiation field that the maser gives rise to. While maser polarization is a powerful tool to trace magnetic field structures in regions and at densities where no other tracers are available, modeling efforts have not been able to fully explain the features of the emergence of this polarization in a comprehensive model.

It is usual to represent the maser system as a two-level system. Each level is split up into its magnetic sublevels, that may be shifted in energy from each other by the Zeeman effect. A level of angular momentum j is subsequently split up into $2j+1$ magnetic sublevels, that are shifted in energy $E_{jm} = E_j + \mu_N B g_j m$, where μ_N is the nuclear magneton, B is the magnetic field, and g_j is the level specific g-factor. Note that we are modeling a diamagnetic molecule in this example; for a paramagnetic molecule, the Zeeman effect would scale with the Bohr magneton μ_B. The shift in energy of the magnetic sublevels of the maser transitions due to the Zeeman effect subsequently shifts the frequency associated with the magnetic subtransitions of the maser transition $\nu(m,m') = \nu_0 + \frac{\mu_N}{h} B[g_j m - g_{j'} m']$, where ν_0 is the transition frequency at $B=0$, and j' is the lower level, with associated magnetic quantum number m'. Selection rules allow only for the $\Delta m = m - m' = \pm 1, 0$ transitions that are the $\sigma^{\pm}$ and π^0 transitions. When the magnetic field is along the line-of-sight, the $\sigma^{\pm}$ are the only allowed transitions and are associated with an adverse circular polarization. Then, the circular polarization, $V \propto \sigma^+ - \sigma^-$, or following (Lankhaar & Teague 2023), $V \simeq \frac{\mu_N}{h} \bar{g} B_{\rm los} \frac{dI}{d\nu} = \frac{z B_{\rm los}}{2} \frac{dI}{d\nu}$, where I is the Stokes I total intensity of the maser line, and z is the Zeeman coefficient that is

dependent on the transition g-factor, $\bar{g}$, that may be computed from the upper and lower level g-fators (see, Vlemmings *et al.* 2020 for the procedure). The relation between the circular polarization, the z-factor and the line-of-sight component of the magnetic field has been useful to derive magnetic field strengths in star-forming regions (e.g. Lankhaar *et al.* 2018), towards evolved stars (e.g. Vlemmings *et al.* 2006) as well as in OH megamaser galaxies (e.g. Robishaw *et al.* 2008).

When the magnetic field is directed with an angle with respect to line-of-sight, both the $\sigma^{\pm}$ and the π^0 are allowed transitions. The sum of the $\sigma^{\pm}$ transitions add up to match the line-strength of the π^0 transitions. Since $\sigma^{\pm}$ and π^0 transitions are associated with linear polarization, respectively, perpendicular and parallel to the plane-of-the-sky component of the magnetic field, one expects for small Zeeman splittings (with respect to the line-width), that the total linear polarization averages to zero. This is indeed the case if the magnetic sublevels of each maser state are equally populated. However, when magnetic sublevels are populated unequally, a net linear polarization is produced.

An imbalance in the population of magnetic sublevels can be produced for masers in either of two ways. The first case is the saturated maser, whose rate of stimulated emission exceeds the rate of decay of the maser levels. In this case, the different propensities of the $\sigma^{\pm}$ and π^0 transition groups come to expression in the sublevel populations. From both analytical and numerical modeling, it turns out that when the magnetic field projection angle, θ is smaller than the magic angle, or the Van Vleck angle, $\theta_m \approx 54.7^o$, then a net polarization parallel to the magnetic field is produced, while for other angles, polarization perpendicular to the magnetic field is produced. We call the production of maser polarization through this mechanism: maser saturation polarization. The second case is a result of the differential pumping of the magnetic sublevels. In that case, polarization can be produced for any saturation degree. This polarization mechanism is called 'anisotropic pumping'. The relation between the magnetic field and the polarization vector is a function of the anisotropy of the pumping, However, first-principle calculations that quantify anisotropic pumping have not yet been developed, and rather, this mechanism is invoked from phenomenological arguments.

The most salient example of an anisotropically pumped maser are SiO masers excited in the extended atmosphere of evolved stars. The maser transitions occur primarily in the vibrationally excited states, which are excited by the IR radiation from the central star. Since this exciting radiation comes primarily from one direction, i.e. is anisotropic, excitation to the magnetic sublevels is unequal. This naturally leads to anisotropically pumped masers. Similarly, when masers are excited in an anisotropic geometry, such as a shock, the radiation field that is generated by the maser molecule is also anisotropic. Under the right conditions, the anisotropy of the radiation field can significantly manifest in the maser states, thus leading to an anisotropically pumped maser. Collisional interactions often quench the anisotropy on the account that they occur isotropically. Collisions (between neutral species) in a gas with a scalar temperature do not have a preferred direction (Lankhaar & Vlemmings 2020b).

2. A comprehensive model of maser polarization

To move past a phenomenological representation of the anisotropic pumping of masers, we construct a comprehensive model of maser polarization. In it, we divide the maser polarization modeling in two steps. First, we perform an excitation modeling, where we relax the common assumption of equally populated magnetic sublevels. Second, we perform the maser polarization radiative transfer of a two-level maser system (Lankhaar & Vlemmings 2019), where we use the relevant pumping- and decay-operators from our earlier excitation modeling.

https://doi.org/10.1017/S1743921323002429 Published online by Cambridge University Press

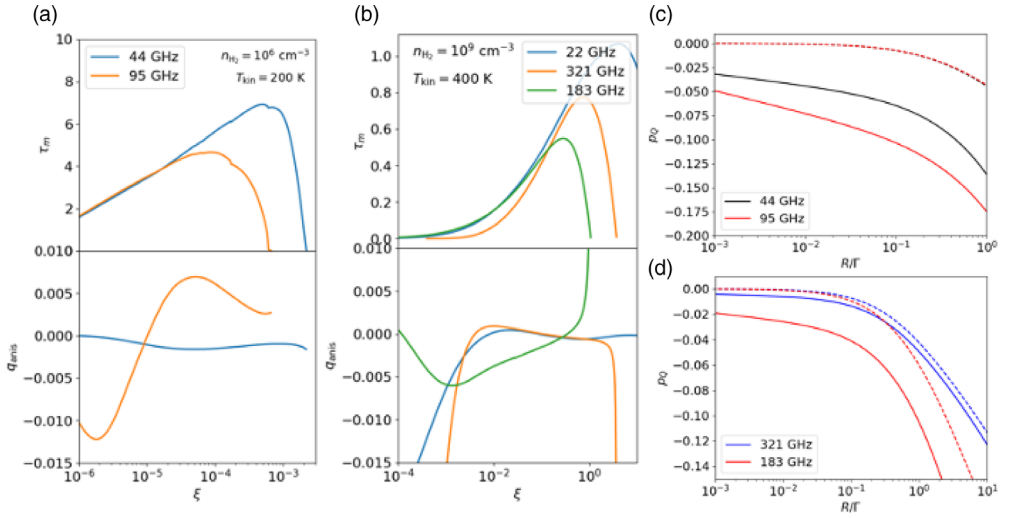

Figure 1. (Anisotropic) pumping parameters of methanol (a) and water (b) masers from polarization resolved excitation modeling. Polarization fractions of methanol (c) and water (d) maser species from polarized radiative transfer simulations using the input of polarization resolved excitation modeling.

To perform the excitation modeling we used PORTAL (Lankhaar & Vlemmings 2020b) in an anisotropic LVG (large velocity gradient) geometry, while fully modeling the magnetic sublevels of all states involved in the excitation, and the two polarization modes of the radiation field. We use an irreducible tensor formalism to afford us a reduction in dimensionality at minimal costs to the accuracy (for a discussion, see Lankhaar & Vlemmings 2020b).

The results of the excitation modeling yield (unsaturated) propagation coefficients that are characterized by isotropic and anisotropic parts. For unsaturated masers, the production of linear polarization may be easily represented by, $p_Q^{\rm anis} \simeq \tanh\left[-\tau_{\rm maser} q_{\rm anis} \sin^2\theta\right] \approx -\tau_{\rm maser} q_{\rm anis} \sin^2\theta$, where the last approximation is valid for polarization degrees $< 10\%$, $\tau_{\rm maser}$ is the maser optical depth and $q_{\rm anis}$ is the maser anisotropy factor. When the maser saturates, this approximation has to be abandoned in favor of rigorous maser polarization modeling, as can be performed with CHAMP (Lankhaar & Vlemmings 2019), that uses the input that can be extracted from the excitation modeling.

3. Simulations

We modeled the excitation of water masers, class I methanol masers, and SiO masers. We modeled all of these species in a plane-parallel like LVG geometry with an aspect ratio of 10, where the velocity gradient follows $\lambda(\mu) = \lambda[\mu^2 + (1-\mu^2)/10]$, where λ is the general velocity gradient and μ is the projection onto the symmetry axis. This is representative for the shock and expanding envelope environments that these masers are excited in. To model the SiO masers, we included the radiation field from a 2000 K stellar object, where we put the maser at 3 stellar radii away from the star.

Methanol masers: 44 GHz polarization vs 95 GHz polarization. There are many class I methanol maser transitions, but in the interest of space, we only compare our results with maser polarization observations of the 44 GHz and 95 GHz methanol masers. Kang *et al.* 2016 quantified the linear polarization of 44 GHz and 95 GHz methanol masers towards high mass star forming regions, and find that for co-spatial masers, the

https://doi.org/10.1017/S1743921323002429 Published online by Cambridge University Press

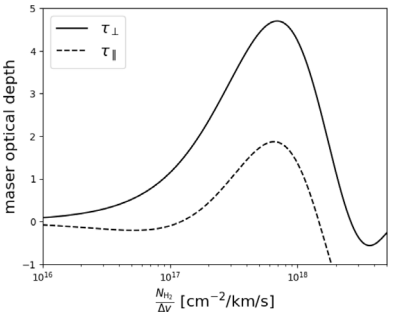

Figure 2. SiO maser optical depth of the radiation component perpendicular and parallel to the magnetic field.

95 GHz transition is more polarized, by a factor up to 3, compared to 44 GHz transition. Since most class I methanol masers are believed to be unsaturated, their polarization is likely due to anisotropic pumping as a result of the shock geometry they are excited in. In Figure 1a, we plot the anisotropic pumping factor, $q_{\rm anis}$, for typical excitation conditions of $T_{\rm kin} = 200$ K and $n_{\rm H_2} = 10^6$ cm^{-3}, for a range of specific column densities (we use the metric ξ for specific column densities, for more discussion, see Leurini *et al.* 2016). We find that the 95 GHz transition has significant anisotropic pumping, while the anisotropic pumping is rather weak for 44 the GHz transition. When we use the results of our excitation analysis as the input for a polarized maser radiative transfer simulation, we find that—for the same degree of saturation, R/Γ—that the 95 GHz maser is about twice as strongly polarized as the 44 GHz maser.

Water masers. Water masers are often found to be significantly polarized. Of the water maser transitions, the 22 GHz maser is generally the strongest, and accordingly most searched for its polarization. Some millimeter and sub-millimeter water transitions have recently been uncovered as masers, of which the 183 GHz and 321 GHz masers have been used as extragalactic circumnuclear accretion disk tracers (e.g. Pesce *et al.* 2023). We compare the polarization of these masers according to our modeling. Figure 1b, shows the anisotropic pumping factor, $q_{\rm anis}$, in our model of the maser polarization for typical excitation conditions of $T_{\rm kin} = 400$ K and $n_{\rm H_2} = 10^9$ cm^{-3}, for a range of specific column densities. We find that while anisotropic pumping is present for both the 321 GHz and 22 GHz masers, it is significantly enhanced for the 183 GHz maser. When we use the results of our excitation analysis as the input for a polarized maser radiative transfer simulation, we find that—for the same degree of saturation, R/Γ—that the 183 GHz maser is polarized stronger than the 22 GHz and 321 GHz masers. This is the result of not only the anisotropic pumping, but also of the low angular momentum of the transition, that enhances the polarization due to saturation effects. We find that the 22 GHz water maser shows similar polarization signature when anisotropic pumping is excluded from the maser radiative transfer.

SiO masers. With polarization degrees up to 100 %, SiO masers are the prototypical example of anisotropically pumped masers. We modeled the excitation of SiO masers for typical excitation conditions of $T_{\rm kin} = 1200$ K and $n_{\rm H_2} = 10^{12}$ cm^{-3}, for a range of specific column densities. Figure 2 shows a comparison between the predicted optical depth of the radiation field mode perpendicular and parallel to the projected magnetic field direction for the $J = 1 \rightarrow 0$ transition. We find a significant difference between the optical depth between both radiation modes. In fact, for a significant range of specific column densities, we find that the perpendicular mode is masing, while the parallel radiation mode is in absorption. Such a configuration predicts 100 % polarization for all degrees of saturation. Additionally, it shows the importance of modeling SiO masers

https://doi.org/10.1017/S1743921323002429 Published online by Cambridge University Press

comprehensively, including also the magnetic sublevels in the maser excitation, as large differences in population between them within an energy level can occur.

References

Lankhaar, B., Vlemmings, W. *et al.* 2018, *Nature Astronomy*, 2, 145-150
Lankhaar, B. & Vlemmings, W. 2019, *A&A*, 628, A14
Lankhaar, B. & Vlemmings, W. 2020, *A&A*, 636, A14
Lankhaar, B. & Vlemmings, W. 2020, *A&A*, 638, L7
Vlemmings, W., Lankhaar, B., *et al.* 2019, *A&A*, 624, L7
Lankhaar, B. & Teague, R. 2023, *accepted to A&A*
Vlemmings, W., Diamond, P. & Imai, H. 2006, *Nature*, 440, 58
Robishaw, T., Quataert, E. & Heiles, C. 2008, *ApJ*, 680, 981
Pesce, D., Braatz, J., *et al.* 2023, *ApJ*, 948, 134
Kang, J., Byun, DY., *et al.* 2016, *ApJS*, 227(2), 17
Leurini, S., Menten, K. & Walmsley, C. 2016, *A&A*, 592, A31

https://doi.org/10.1017/S1743921323002429 Published online by Cambridge University Press